Letter | Editors' Suggestion

Probing superconductivity with tunneling spectroscopy in rhombohedral graphene

Denis Sedov and Mathias S. Scheurer
Institute for Theoretical Physics III, University of Stuttgart, 70550 Stuttgart, Germany

(Received 1 April 2025; revised 18 March 2026; accepted 2 April 2026; published 28 April 2026)

Motivated by experiments on rhombohedral tetralayer graphene showing signs of superconductivity emerging from a valley-polarized normal state, we here analyze theoretically how tunneling spectroscopy can be used to probe the superconducting order parameter of the system. To describe different pairing scenarios on equal footing, we develop a microscopic tunneling approach that can capture arbitrary, including finite-momentum, superconducting order parameters and low-symmetry normal-state Hamiltonians. Our analysis shows that the broken time-reversal symmetry in a single valley leads to unique features in the weak-tunneling regime that are different for commensurate and incommensurate Cooper pair momenta. We further uncover an unconventional spatial dependence of the Andreev conductance, allowing to distinguish between three topologically distinct classes of single-**q** pairing states in the system, and compute the signatures of a competing translational-symmetry breaking three-**q** superconductor.

DOI: 10.1103/6qg4-cfgc

Introduction. In recent years, multilayer graphene systems have been established as a fascinating route to complex correlated physics [1–6]. In addition to other interaction-induced phases, such as spontaneous polarization of the different internal "flavor" degrees of freedom [5–9], the fact that these systems host superconducting states [6,10] has been a particularly strong driving force of research. Although tunneling experiments hint at pairing beyond the simple BCS paradigm in twisted multilayer graphene [11–19], the form of the superconducting order parameter and the pairing glue are still the subject of debate. After the discovery [6] and subsequent theoretical study [20–30] of superconductivity in rhombohedral stacks of graphene, see Fig. 1(a), very recently, an experiment [31] revealed a rather remarkable behavior in rhombohedral tetralayer graphene (RTG); here, superconductivity seems to be born out of a valley-polarized normal state, i.e., the normal-state Fermi surfaces are exclusively located in the vicinity of the **K** and not the **K**′ point (or vice versa). For one of the two valley-polarized superconductors, the spin degree of freedom is also likely polarized. Multiple works studying the energetics and properties of superconductivity in valley-imbalanced systems [32–44] demonstrate that the lack of orbital time-reversal symmetry (TRS) in the normal state can lead to exotic physical properties.

As a clear experimental identification of the form of superconductivity is typically very challenging, this work explores theoretically how tunneling spectroscopy can be used to gain crucial information about pairing in valley-polarized RTG. This is a complex endeavor because a sufficiently large valley polarization is not only expected to lead to $\mathbf{q} = 0$ intravalley pairing, i.e., Cooper pairs with a commensurate center-of-mass momentum $2\mathbf{K}$, but also to states with incommensurate momentum $2\mathbf{K} + \mathbf{q}$, where $\mathbf{q} \neq 0$ [32]. Furthermore, the off-resonant band energies of the paired electrons lead to nodal or fully gapped regimes [33–39], depending on the size of the order parameter, and, for $\mathbf{q} = 0$, one has to distinguish pairing in the three distinct irreducible representations (IRs) A, E, E^* of the point group C_3 generated by threefold rotational symmetry C_{3z} (all IRs are one dimensional since C_3 is Abelian); at $\mathbf{q} \neq 0$ these states can still be distinguished based on their Chern number. Finally, Ref. [39] showed that apart from the aforementioned single-**q** states, also three-**q** states are possible which restore C_{3z} but break translational symmetry. We here demonstrate that—taking advantage of the unique features of intravalley pairing—a combination of weak- and strong-tunneling measurements at different high-symmetry positions will provide key insights about which of the above-mentioned pairing states is present in the system.

General formalism. To model tunneling experiments in RTG systematically, we incorporate and generalize the Hamiltonian approach to tunneling based on the Keldysh formalism [45] to the case with arbitrary momentum dependent superconducting (SC) order parameters $\Delta_{\mathbf{k},-\mathbf{k}'}$, coupling electronic states at in general nonzero net momentum, $\mathbf{k} - \mathbf{k}' \neq 0$, and without TRS in the multicomponent normal-state Bloch Hamiltonian $h_{\mathbf{k}}$. More explicitly, the target system, here RTG, is described by $\hat{H}_c = \sum_{\mathbf{k}} (c^\dagger_{\mathbf{k},\uparrow} h_{\mathbf{k}} c_{\mathbf{k},\uparrow} - c_{-\mathbf{k},\downarrow} \cdot h^{\mathrm{T}}_{-\mathbf{k}} \cdot c^\dagger_{-\mathbf{k},\downarrow}) + \sum_{\mathbf{k},\mathbf{k}'} (c^\dagger_{\mathbf{k},\uparrow} \cdot \Delta_{\mathbf{k},-\mathbf{k}'} \cdot c^\dagger_{-\mathbf{k}',\downarrow} + \mathrm{H.c.})$, where $h_{\mathbf{k}}$ is the continuum eight-band model [46,47] of RTG and $c^\dagger_{\mathbf{k},\sigma}$ is a creation operator of electrons in the **K**-valley with momentum $\mathbf{k}$ and spin σ. We assume that the tunneling is local with respect to the lead degrees of freedom, $\hat{H}_t = \sum_{\mathbf{k},\sigma} f^\dagger_\sigma(0) t^\dagger_{\mathbf{k}} c_{\mathbf{k},\sigma} + \mathrm{H.c.}$, where $f^\dagger_\sigma(0)$ creates an electron at the tip of the lead of a scanning tunneling microscope setup or at the outer atomic layer of a tunnel junction; $t_{\mathbf{k}}$ are the associated (in general matrix-valued) tunneling matrix elements. We also assume

Published by the American Physical Society under the terms of the Creative Commons Attribution 4.0 International license. Further distribution of this work must maintain attribution to the author(s) and the published article's title, journal citation, and DOI.

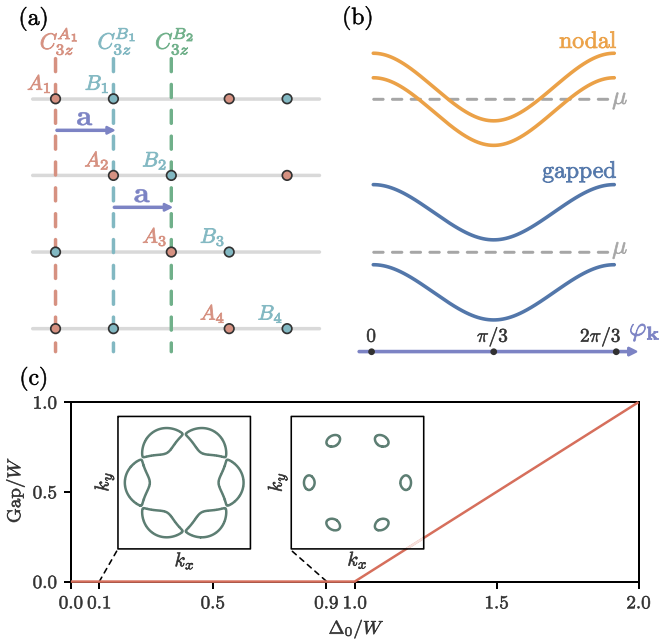


FIG. 1. (a) Schematic illustration of the geometry of RTG; A_n, B_n are sublattice atoms of the nth graphene layer. (b) Bogoliubov excitation spectrum along the contour $\xi_{\mathbf{k}} + \xi_{-\mathbf{k}} = 0$ in the nodal and gapped regimes. (c) Dependence of the excitation gap on the magnitude of $|\Delta_{\mathbf{k}}| = \Delta_0$ for the toy-model dispersion $\xi_{\mathbf{k}} = \mathbf{k}^2/(2m) + W\cos(3\varphi_{\mathbf{k}})$; for completeness, we also present the nodal lines of the Bogoliubov excitations for two values of Δ_0/W in the gapless regime.

that both systems are kept at the same temperature and the difference between their chemical potentials is controlled by the bias voltage eV. Thus, we neglect any effects of the distribution function renormalization.

The tunneling current can be divided into four distinct terms with different physical interpretations ([45], see Supplemental Material (SM) [48] for a detailed derivation). While we always include all of them in our numerics, for our discussion here, only two of them are crucial. First, in the weak-tunneling regime, when tunneling amplitudes are much smaller than characteristic energies of the systems (e.g., bandwidth, hopping constants), the current is mostly determined by the famous expression, $I_{\text{weak}} \sim \int d\omega \rho_{f,\text{pp}}(\omega - eV) \sum_{\mathbf{k},\mathbf{k}'} t^{\dagger}_{\mathbf{k}} \rho_{c,\text{pp}}(\omega, \mathbf{k}, \mathbf{k}') t_{\mathbf{k}'} [n_{\text{F}}(\omega - eV) - n_{\text{F}}(\omega)] + o(\|t\|^2)$, where $\rho_{f/c,pp}$ are bare particle spectral functions and we focused on a single channel in the lead. The corresponding tunneling conductance, $G(eV) = \partial I/\partial(eV)$, is then proportional to the local density of states (LDOS). Therefore, weak-tunneling allows to probe spectral features of the Bogoliubov excitations. Second, when tunneling amplitudes become large enough, the Andreev contribution to the current become non-negligible. It is proportional to the SC order parameter $\Delta_{\mathbf{k},-\mathbf{k}'}$ and reads as

$$I_{\text{A}} = \frac{4\pi e}{\hbar} \int d\omega \left| \sum_{\mathbf{k},\mathbf{k}'} t^{\dagger}_{\mathbf{k}} G^{r}_{cc,\text{ph}}(\omega, \mathbf{k}, \mathbf{k}') t^{*}_{-\mathbf{k}'} \right|^2 \rho^{\text{pp}}_{f}(\omega - eV) \times \rho^{\text{hh}}_{f}(\omega + eV)[n_{\text{F}}(\omega - eV) - n_{\text{F}}(\omega + eV)], \quad (1)$$

where $G^{r}_{cc,\text{ph}} \propto \Delta_{\mathbf{k},-\mathbf{k}'}$ is the particle-hole (anomalous) part of the retarded Green's function of the RTG in the Nambu basis. The Andreev current is generated in the process in which electrons tunnel from the lead to the SC, then by the Andreev scattering are converted to a hole tunneling back to the lead. This is the only contribution to the current that does not generally vanish when $|eV|$ lies within the gap of the Bogoliubov excitations. This feature along with its proportionality to the SC order parameter makes the strong tunneling regime a useful tool to extract information about the symmetry of the SC from tunneling experiments.

Weak tunneling. We begin our analysis in the weak-tunneling regime, where the current is dominated by I_{weak} following the LDOS. We further first focus on $\mathbf{q} = 0$ intravalley pairing (commensurate momentum $2\mathbf{K}$) in valley-polarized RTG and only keep the band crossing the Fermi level. Then superconductivity is described by $H_{1\text{b}} = \sum_{\mathbf{k},\sigma} \xi_{\mathbf{k}} d^{\dagger}_{\mathbf{k},\sigma} d_{\mathbf{k},\sigma} + H_{\Delta}$, where $H_{\Delta} = \sum_{\mathbf{k}} (d^{\dagger}_{\mathbf{k},\uparrow} \Delta_{\mathbf{k}} d^{\dagger}_{-\mathbf{k},\downarrow} + \text{H.c.})$ and $d^{\dagger}_{\mathbf{k},\uparrow\downarrow}$ are electronic creation operators in the active band hosting superconductivity.

To gain intuition, we first consider the corresponding Bogoliubov spectrum, given by $E^{\pm}_{\mathbf{k}} = 1/2(\xi_{\mathbf{k}} - \xi_{-\mathbf{k}} \pm \sqrt{(\xi_{\mathbf{k}} + \xi_{-\mathbf{k}})^2 + 4|\Delta_{\mathbf{k}}|^2})$. Broken TRS, $\xi_{\mathbf{k}} \neq \xi_{-\mathbf{k}}$, results in two pairing regimes—nodal and fully gapped—controlled by the magnitude $|\Delta_{\mathbf{k}}|$ of the order parameter, which we set to be $\mathbf{k}$ independent, $\Delta_0 = |\Delta_{\mathbf{k}}|$, for simplicity of the following discussion. This behavior can be understood by considering a toy-model dispersion capturing the TRS-breaking trigonal warping $\xi_{\mathbf{k}} = \mathbf{k}^2/(2m) + W\cos(3\varphi_{\mathbf{k}}) - \mu$ (w.l.o.g. $W > 0$), which leads to the following dispersion of the Bogoliubov bands, $E^{\pm}_{\mathbf{k}} = W\cos(3\varphi_{\mathbf{k}}) \pm \sqrt{(\mathbf{k}^2/(2m) - \mu)^2 + \Delta_0^2}$. We see that the gap depends on the ratio between Δ_0 and the magnitude of the TRS-breaking part of the dispersion; it is given by $\max(0, \Delta_0 - W)$ in this case. $E^{\pm}_{\mathbf{k}}$ has six distinct stationary points located on the symmetrized Fermi surface, $\xi_{\mathbf{k}} + \xi_{-\mathbf{k}} = 0$, at angles $\varphi = \pi m/3$, $m \in \mathbb{Z}$—three saddle points and three minima (maxima). In Fig. 1(b), we present the angular dependence of Bogoliubov spectrum of the toy model along the contour $\xi_{\mathbf{k}} + \xi_{-\mathbf{k}} = 0$, and note that the bands behave quadratically in the direction perpendicular to this contour; Figure 1(c) shows the dependence of the excitation gap on the magnitude of the SC order parameter, and nodal lines of the excitations for two values of Δ_0/W. The stationary points of the excitation spectrum lie on the symmetrized Fermi surface $\xi_{\mathbf{k}} + \xi_{-\mathbf{k}} = 0$ also beyond the toy model as long as the TRS-breaking part of the one-particle energy, $\xi_{\mathbf{k}} - \xi_{-\mathbf{k}}$, depends only on the direction of $\mathbf{k}$. Although the dispersion of the RTG does not have this strict property, we find that the toy model captures all the main features present in the numerical results.

The discussed behavior is visible in the weak-tunneling conductance, shown in Fig. 2(b). Sharp peaks correspond to log divergences of the DOS related to the aforementioned saddle points of $E^{\pm}_{\mathbf{k}}$. In contrast to the intervalley pairing in Fig. 2(a), these peaks do not appear at the edges of the hard gap, but above it. In the gapped intravalley pairing case, in the vicinity of the hard gap energy, which is smaller than the order-parameter magnitude Δ_0 [18], the spectrum $E^{\pm}_{\mathbf{k}}$ behaves quadratically in $\mathbf{k}$. This leads to a steplike behavior of the

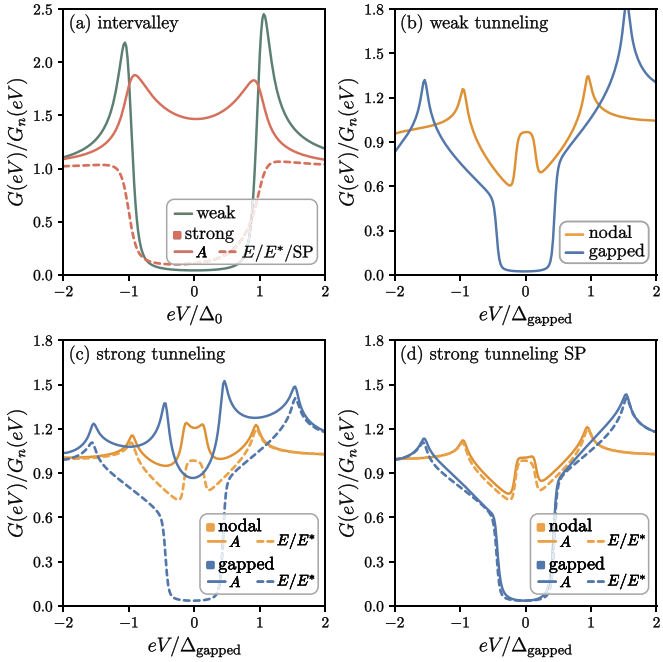


FIG. 2. Normalized tunneling conductance for tunneling into the A_1 sublattice in different regimes. (a) The tunneling conductance in the weak and strong tunneling regime for single-band intervalley pairing in RTG. (b) Weak tunneling conductance in valley-polarized RTG. (c) and (d) present the strong tunneling conductance for spin-singlet and spin-polarized intravalley pairing, respectively. Weak tunneling conductance is the same for all IRs of the order parameter. Changing the tip position from A_1 to B_1 (or B_2) essentially results in the cyclic permutation of the curves of the strong tunneling conductance in (c) and (d). The intervalley case (a), however, is qualitatively independent of the tip position. Lifetime broadening $\eta/\Delta_{\text{gapped}} = 0.015$, temperature $T/\Delta_{\text{gapped}} = 0.015$, $\Delta_{\text{gapped}}/\Delta_{\text{nodal}} = 2.5$, $|t^2_{\text{weak}}\rho_{f,n}(0)\rho_{c,n}(0)| = 0.25 \times 10^{-3}$, $|t^2_{\text{strong}}\rho_{f,n}(0)\rho_{c,n}(0)| = 2.5$, where $\rho_{f/c,n}(0)$ are the normal LDOS of the system, Δ_{gapped} and Δ_{nodal} are the magnitudes of the SC order parameter in the gapped and nodal regimes, respectively.

tunneling conductance instead of the usual "coherence peaks". The nodal regime is characterized by a finite-height plateau near the Fermi energy, almost coinciding with the normal tunneling conductance. We note that additional spin polarization in the normal state does not change these conclusions, because the DOS depends only on the magnitude of $\Delta_{\mathbf{k}}$. It is worth adding that in the time-reversal symmetric case the nodal nature of the Bogoliubov excitation is usually a consequence of nodes of the SC order parameter, near which the Bogoliubov quasiparticles exhibit linear dispersion leading to the V-shape DOS. Here, the crossover between nodal and gapped regimes comes purely from the energy mismatch, $\xi_{\mathbf{k}} \neq \xi_{-\mathbf{k}}$.

Strong tunneling. The weak-tunneling regime gives access to unique features associated with broken TRS in RTG, but it is not sensitive to the phase of $\Delta_{\mathbf{k}}$ and, thus, the IR of the order parameter. This is different in the strong-tunneling regime, where I_{A} in Eq. (1) can become dominant. To show this, we choose a gauge in which $d_{\mathbf{k}}$ transform trivially under threefold rotations around A_1 [see Fig. 1(a)], without acquiring a phase, $C^{A_1}_{3z} : d^\dagger_{\mathbf{k}} \to d^\dagger_{C_{3z}\mathbf{k}}$. We then associate the phase factor $w = 1, e^{2\pi i/3}, e^{-2\pi i/3}$ in the action of $C^{A_1}_{3z}$ on the order parameter, $\Delta_{\mathbf{k}} \to \Delta_{C^{-1}_{3z}\mathbf{k}} = w\Delta_{\mathbf{k}}$, with IRs A, E, E^*, respectively [49]. Although other choices are also possible (cf. other rotation axes below), we here use this convention for the following reason: In general, one can split the Berry curvature of the superconductor into three contributions, $\Omega = \Omega_{\text{SC}} + \Omega_{\text{b}} + \delta\Omega$ (see SM [48]). Here, Ω_{SC} is the Berry curvature of the Bogoliubov Hamiltonian of the single-band model $H_{1\text{b}} = \sum_{\mathbf{k}} \Psi^\dagger_{\mathbf{k}} h_{\text{BdG}}(\mathbf{k}) \Psi_{\mathbf{k}}$, with Nambu spinor $\Psi_{\mathbf{k}}$, i.e., $\Omega_{\text{SC}} = \mathbf{g}_{\mathbf{k}} \cdot (\partial_x \mathbf{g}_{\mathbf{k}} \times \partial_y \mathbf{g}_{\mathbf{k}})/(2|\mathbf{g}_{\mathbf{k}}|^3)$ where $h_{\text{BdG}}(\mathbf{k}) = E_0(\mathbf{k})\tau_0 + \mathbf{g}_{\mathbf{k}} \cdot (\tau_x, \tau_y, \tau_z)^T$; alternatively, one can rewrite it as $\Omega_{\text{SC}} = -2\,\text{Im}[(\partial_x \mathbf{a}^*_{\mathbf{k}}) \cdot \partial_y \mathbf{a}_{\mathbf{k}}]$, where $\mathbf{a}_{\mathbf{k}}$ are the (two-component) eigenstates of the lower band of h_{BdG}. Furthermore, Ω_{b} is the contribution from the Berry curvature of the bands we study pairing in and $\delta\Omega$ a term involving both, which restores gauge invariance; while Ω_{b} and Ω are gauge-invariant separately, Ω_{SC} is not, since $d_{\mathbf{k}} \to e^{i\varphi_{\mathbf{k}}} d_{\mathbf{k}}$ will add a $\mathbf{k}$-dependent phase to $\Delta_{\mathbf{k}}$, affecting the $\mathbf{k}$-dependence of $\mathbf{g}_{\mathbf{k}}$ and $\mathbf{a}_{\mathbf{k}}$. The required gauge invariance of $\Omega_{\text{SC}} + \delta\Omega$ can be made manifest by introducing the gauge-covariant derivative in particle-hole space,

$$D_j = \tau_0 \partial_j + \begin{pmatrix} \langle \phi_{\mathbf{k},+} | \partial_j \phi_{\mathbf{k},+} \rangle & 0 \\ 0 & \langle \phi_{\mathbf{k},-} | \partial_j \phi_{\mathbf{k},-} \rangle \end{pmatrix}, \tag{2}$$

where $|\phi_{\mathbf{k},+}\rangle = |u_{\mathbf{k}}\rangle$, $|\phi_{\mathbf{k},-}\rangle = |u^*_{-\mathbf{k}}\rangle$. This allows us to write $\Omega_{\text{SC}} + \delta\Omega = -2\,\text{Im}[(D_x \mathbf{a}^*_{\mathbf{k}}) \cdot D_y \mathbf{a}_{\mathbf{k}}]$.

It is straightforward to show that, for the Bloch bands of a minimal two-band model [47] of RTG, the contributions of Ω_{b} and $\delta\Omega$ to the Chern number C of the superconductor cancel out with the contribution coming from higher energies beyond the continuum model in the above-mentioned gauge where $C^{A_1}_{3z}$ acts trivially. As detailed in the SM [48], this holds under the natural assumption that the emergence of valley polarization only leads to an energetic deformation of the full band in the Brillouin zone of the underlying lattice model and not to a topological gap closing with other remote bands. We then simply have $C = \frac{1}{2\pi} \int \mathrm{d}^2\mathbf{k}\, \Omega_{\text{SC}}$ such that the A state with $\Delta_{\mathbf{k}} = \Delta_0$ and E/E^* state with $\Delta_{\mathbf{k}} = \Delta_0 e^{\pm i\varphi_{\mathbf{k}}}$ are topologically trivial, $C = 0$, and nontrivial with $C = \pm 1$, respectively.

For these order parameters and taking a spin-unpolarized normal state, we show the conductance in the strong-tunneling regime in Fig. 2(c) when tunneling exclusively into the A_1 sublattice. We can see that the result for E/E^* now differs significantly from that of A, since the former only exhibits slight modifications in the normalized conductance compared to weak tunneling, while the latter behaves rather differently. Most notably, in the gapped regime, only A exhibits a sizable Andreev signal below the gap. This can be straightforwardly understood by noting that the $\mathbf{k}$ sum in Eq. (1) vanishes by symmetry. This results from the fact that tunneling and thus $t_{\mathbf{k}}$ respect $C^{A_1}_{3z}$ while $\Delta_{\mathbf{k}}$ transforms nontrivially under it for E and E^* pairing, i.e., this holds as long as the tunnel process preserves $C^{A_1}_{3z}$.

Apart from $C^{A_1}_{3z}$, RTG has two additional rotational symmetries, $C^{B_1}_{3z}$ and $C^{B_2}_{3z}$, as shown in Fig. 1(a). As they are related by lattice translational symmetry, it holds $C^M_{3z} : d^\dagger_{\mathbf{k}} \to \gamma_M e^{i\mathbf{a}_M(\mathbf{k}-C_{3z}\mathbf{k})} d^\dagger_{C_{3z}\mathbf{k}}$ with $\mathbf{a}_M = 0, \mathbf{a}, 2\mathbf{a}$ and phases $\gamma_M = 1, e^{-2\pi i/3}, e^{2\pi i/3}$ for $M = A_1, B_1, B_2$; the phases cancel out

in an intervalley superconducting order parameter, which thus transforms identically under all of them. In contrast, this is not the case for our intravalley superconductor which carries finite, lattice-commensurate momentum, $C_{3z}^{M}:\Delta_{\mathbf{k}}\to\gamma_M^2\Delta_{C_{3z}^{-1}\mathbf{k}}=\gamma_M^2 w\Delta_{\mathbf{k}}$. Therefore, e.g., the A state defined above transforms under IR E and E^* with respect to $C_{3z}^{B_1}$ and $C_{3z}^{B_2}$. This is of direct experimental relevance since changing the tip position from A_1 to $B_{1,2}$ will break $C_{3z}^{A_1}$ symmetry in $t_{\mathbf{k}}$ and, instead, $C_{3z}^{B_{1,2}}$ will be preserved. As such, moving the tip position will lead to a cyclic permutation of which of the three superconductors with Chern number $C=0,\pm1$ exhibits the Andreev peak. Consequently, Andreev spectroscopy at multiple tip positions will yield crucial, phase-sensitive information about the superconductor, which is unique to intravalley pairing. In constrast, the strong tunneling conductance in the intervalley case, Fig. 2(a), is qualitatively independent of the tip position since the order parameter transforms under the same IR of $C_{3z}^{M},\forall M$. Note, however, that the magnitude of the normal tunneling conductance changes since the lowest band is mostly polarized in the A_1-B_4 subspace.

We finally mention that additional full spin polarization of the normal state will generally lead to a suppression of the Andreev conductance (in the local tunneling approximation) even for the trivial IR of the order parameter, which we also show in Fig. 2(d). For E/E^* IRs, the Andreev signal vanishes because of the same above-mentioned argument. As follows again from the $\mathbf{k}$ sum in Eq. (1), the A IR spin-polarized (SP) Andreev signal has to vanish at $eV=0$ due to the fermionic antisymmetry, $\Delta_{\mathbf{k}}=-\Delta_{-\mathbf{k}}$, but is finite for $eV\neq0$. This is to be contrasted with spin polarization in intervalley single-band pairing, where TRS implies $I_{\mathrm{A}}=0$ for *all* energies and IRs (see SM [48]).

Finite momentum pairing. Although C_{3z}^{M} can pin $\mathbf{q}$ to zero for an extended set of parameters [32], broken TRS can also lead to pairing at incommensurate momenta, i.e., $\mathbf{q}\neq0$ in $H_\Delta=\sum_{\mathbf{k}}d^\dagger_{\mathbf{k}+\mathbf{q}/2,\uparrow}\Delta_{\mathbf{k}}d^\dagger_{-\mathbf{k}+\mathbf{q}/2,\downarrow}$ in $H_{1\mathrm{b}}$, which we refer to as single-$\mathbf{q}$ pairing. This breaks C_{3z} symmetry, but we can still use the Chern number C and adiabatic connectivity to the $\mathbf{q}=0$ states above to distinguish the pairing states [39]. Focusing on the fully gapped regime (see SM [48] for nodal pairing), we present in Fig. 3 the tunneling conductance for $\mathbf{q}\neq0$. In the weak-tunneling regime, Fig. 3(a), we see that the hard gap is reduced when $\mathbf{q}\neq0$, while the overall region of LDOS suppression increases. This is related to the fact that the $\mathbf{q}$-induced shifts of the particle and hole Fermi surfaces in Fig. 1(b) lead to an increase of "particle-hole nesting" (and, thus, of the gap) in some part of $\mathbf{k}$ space at the expense of other regions. Another manifestation of finite $\mathbf{q}$ in Fig. 3(a) is the splitting of the Van Hove peaks into two less pronounced peaks. Here we chose the direction of $\mathbf{q}$ along the mirror-symmetry axes of the spectrum, which is energetically favored in most parameter regimes [39].

In Fig. 3(b), we compare the weak- and strong-tunneling conductance for different IRs of the order parameter and tunneling to the A_1 sublattice. As finite $\mathbf{q}$ breaks the C_{3z} symmetry, it is expected to lead to a nonvanishing subgap Andreev current for all IRs. Even though the magnitude of $\mathbf{q}$ we chose leads to a significant reduction of the gap in the weak-tunneling limit, the qualitative behavior of the pairing is

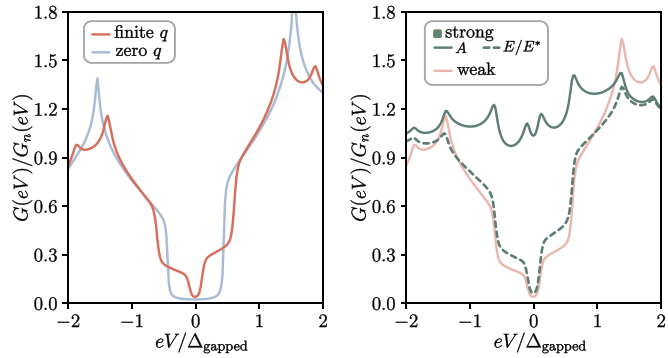


FIG. 3. Tunneling conductance of the finite-momentum single-$\mathbf{q}$ state. (a) Comparison of the weak tunneling conductance between zero-q and finite-q SC. (b) Comparison between weak and strong tunneling conductance of the finite-q SC for different IRs of the SC order parameter. Weak tunneling conductance is independent of the IRs of the order parameter. $\eta/\Delta_{\mathrm{gapped}}=0.015$, $T/\Delta_{\mathrm{gapped}}=0.015$, $|t^2_{\mathrm{weak}}\rho_{f,n}(0)\rho_{c,n}(0)|=0.25\times10^{-3}$, $|t^2_{\mathrm{strong}}\rho_{f,n}(0)\rho_{c,n}(0)|=2.5$, $\mathbf{q}/\langle k_{\mathrm{F}}\rangle=(0.1,0)$, where $\langle k_{\mathrm{F}}\rangle$ is the angle-averaged absolute value of the Fermi vector.

hardly affected for strong tunneling; we still see a significant difference between A ($\Delta_{\mathbf{k}}=\Delta_0$) and E/E^* ($\Delta_{\mathbf{k}}=\Delta_0e^{\pm i\varphi_{\mathbf{k}}}$) such that the strong-tunneling regime can still be used to distinguish the three different pairing states with Chern numbers $C=0,\pm1$.

Three-$\mathbf{q}$ superconductivity. Despite the finite momentum of the superconductors discussed so far, lattice translation accompanied by an appropriate U(1) gauge transformation is still a symmetry such that any physical observable, like the tunneling conductance, will respect Bravais-lattice translational symmetry. However, it is also possible that a superposition of three C_{3z}-related momenta, $\mathbf{q}_j=C_{3z}^{j-1}\mathbf{q}$, $j=1,2,3$, is stabilized [39]. This three-$\mathbf{q}$ state is characterized by $H_\Delta=\sum_{\mathbf{k}}\sum_{j=1}^{3}d^\dagger_{\mathbf{k}+\mathbf{q}_j/2,\uparrow}\Delta_{C_{3z}^{1-j}\mathbf{k}}d^\dagger_{-\mathbf{k}+\mathbf{q}_j/2,\downarrow}+\mathrm{H.c.}$. It respects C_{3z}^{M} (modulo phase depending on M) but breaks translational symmetry explicitly and leads to a superlattice reconstruction of the continuum bands of RTG; the resulting model is analogous to the continuum model [50,51] of moiré systems but with anomalous momentum-mixing terms.

Since this superconductor can be distinguished from the states discussed earlier by its spatial variation, we only focus on the calculation of the LDOS here, which can be probed in the weak-tunneling regime. In Fig. 4(a), we present the LDOS (projected to the upper layer of RTG) in the emerging superlattice unit cell, at $\omega=0$ and for small $\mathbf{q}$ (much smaller than the Fermi wave vector). Intuitively, for small $\mathbf{q}$, one can think of the system at each position $\mathbf{R}$ locally as a superconductor with gap $\Delta_{\mathbf{k}}(\mathbf{R})=\Delta_{\mathbf{k}}\sum_j e^{i\mathbf{q}_j\mathbf{R}}$, corresponding to a spontaneous vortex-antivortex lattice. This explains why we obtain low LDOS and reduced low-energy spectral weight, see also Fig. 4(b), near $\Gamma_{\mathbf{R}}$ associated with constructive interference of the three phases $e^{i\mathbf{q}_j\mathbf{R}}$ in $\Delta_{\mathbf{k}}(\mathbf{R})$; the destructive interference, on the other hand, leads to a lack of suppression of the LDOS at $\mathrm{K}_{\mathbf{R}}$ (location of the vortices) and $\mathrm{M}_{\mathbf{R}}$.

While there are some subtle differences in the LDOS between the slowly varying local picture and the full model (see SM [48] for details), additional features appear for larger $\mathbf{q}$,

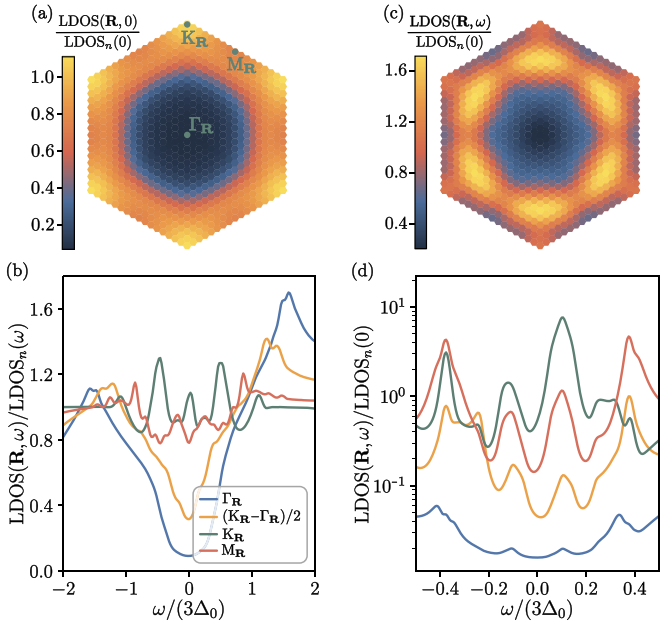


FIG. 4. LDOS of the three-**q** superconductor. (a) Normalized LDOS at the Fermi energy ($\omega = 0$) in the emergent superlattice unit cell in the nodal small-$|\mathbf{q}|$ regime. (b) Energy dependence of the normalized LDOS at the three high-symmetry positions indicated in (a). (c) and (d) show the same in the large-$|\mathbf{q}|$ regime, except that (a) is at $\omega/(3\Delta_0) = 0.64$. We here assume $\Delta_\mathbf{k} = \Delta_0$. In (a) and (b): $\mathbf{q}_1/\langle k_F\rangle = (0.05, 0)$, $\eta/(3\Delta_0) = 0.067$; in (c) and (d): $\mathbf{q}_1/\langle k_F\rangle = (0.3, 0)$, $\eta/(3\Delta_0) = 0.017$.

see Figs. 4(c) and 4(d); this is also the energetically more favorable regime [39] of the three-**q** state. We can see in Fig. 4(d) that the LDOS is more suppressed at $\omega = 0$ for all positions (note the logarithmic scale). Above the gap, we see multiple complex peaks originating from the superlattice reconstruction of the Bogoliubov bands and a nontrivial spatial dependence in the emergent unit cell, see Fig. 4(c).

Conclusion. Our work demonstrates that the broken TRS in valley-imbalanced superconductors leads to a variety of features in tunneling spectroscopy that are different from pairing states emerging out of normal states with TRS. Given the remarkable progress in scanning tunneling studies of correlated graphene systems in recent years [11,12,52–58], we are confident that our formalism and results will provide crucial insights into the microscopic superconducting physics of RTG.

Acknowledgments. M.S.S. thanks Maine Christos and Pietro Bonetti for a collaboration on a related project on RTG [39]. All authors further acknowledge funding by the European Union (ERC-2021-STG, Project No. 101040651—SuperCorr). Views and opinions expressed are however those of the authors only and do not necessarily reflect those of the European Union or the European Research Council Executive Agency. Neither the European Union nor the granting authority can be held responsible for them. M.S.S. is also grateful for support by Grant No. NSF PHY-2309135 for his stay at the Kavli Institute for Theoretical Physics (KITP) where a part of the research was done.

Data availability. The data that support the findings of this article are not publicly available upon publication because it is not technically feasible and/or the cost of preparing, depositing, and hosting the data would be prohibitive within the terms of this research project. The data are available from the authors upon reasonable request.

[1] E. Y. Andrei and A. H. MacDonald, Graphene bilayers with a twist, Nat. Mater. **19**, 1265 (2020).
[2] L. Balents, C. R. Dean, D. K. Efetov, and A. F. Young, Superconductivity and strong correlations in moiré flat bands, Nat. Phys. **16**, 725 (2020).
[3] K. P. Nuckolls and A. Yazdani, A microscopic perspective on moiré materials, Nat. Rev. Mater. **9**, 460 (2024).
[4] P. A. Pantaleón, A. Jimeno-Pozo, H. Sainz-Cruz, V. Phong, T. Cea, and F. Guinea, Superconductivity and correlated phases in non-twisted bilayer and trilayer graphene, Nat. Rev. Phys. **5**, 304 (2023).
[5] H. Zhou, T. Xie, A. Ghazaryan, T. Holder, J. R. Ehrets, E. M. Spanton, T. Taniguchi, K. Watanabe, E. Berg, M. Serbyn, and A. F. Young, Half- and quarter-metals in rhombohedral trilayer graphene, Nature (London) **598**, 429 (2021).
[6] H. Zhou, T. Xie, T. Taniguchi, K. Watanabe, and A. F. Young, Superconductivity in rhombohedral trilayer graphene, Nature (London) **598**, 434 (2021).
[7] D. Wong, K. P. Nuckolls, M. Oh, B. Lian, Y. Xie, S. Jeon, K. Watanabe, T. Taniguchi, B. A. Bernevig, and A. Yazdani, Cascade of electronic transitions in magic-angle twisted bilayer graphene, Nature (London) **582**, 198 (2020).
[8] U. Zondiner, A. Rozen, D. Rodan-Legrain, Y. Cao, R. Queiroz, T. Taniguchi, K. Watanabe, Y. Oreg, F. von Oppen, A. Stern, E. Berg, P. Jarillo-Herrero, and S. Ilani, Cascade of phase transitions and Dirac revivals in magic-angle graphene, Nature (London) **582**, 203 (2020).
[9] E. Morissette, J.-X. Lin, D. Sun, L. Zhang, S. Liu, D. Rhodes, K. Watanabe, T. Taniguchi, J. Hone, J. Pollanen, M. S. Scheurer, M. Lilly, A. Mounce, and J. I. A. Li, Dirac revivals drive a resonance response in twisted bilayer graphene, Nat. Phys. **19**, 1156 (2023).
[10] Y. Cao, V. Fatemi, S. Fang, K. Watanabe, T. Taniguchi, E. Kaxiras, and P. Jarillo-Herrero, Unconventional superconductivity in magic-angle graphene superlattices, Nature (London) **556**, 43 (2018).
[11] M. Oh, K. P. Nuckolls, D. Wong, R. L. Lee, X. Liu, K. Watanabe, T. Taniguchi, and A. Yazdani, Evidence for unconventional superconductivity in twisted bilayer graphene, Nature (London) **600**, 240 (2021).
[12] H. Kim, Y. Choi, C. Lewandowski, A. Thomson, Y. Zhang, R. Polski, K. Watanabe, T. Taniguchi, J. Alicea, and S. Nadj-Perge, Evidence for unconventional superconductivity in twisted trilayer graphene, Nature (London) **606**, 494 (2022).
[13] E. Lake, A. S. Patri, and T. Senthil, Pairing symmetry of twisted bilayer graphene: A phenomenological synthesis, Phys. Rev. B **106**, 104506 (2022).
[14] P. O. Sukhachov, F. von Oppen, and L. I. Glazman, Andreev reflection in scanning tunneling spectroscopy of unconventional superconductors, Phys. Rev. Lett. **130**, 216002 (2023).

[15] H. Sainz-Cruz, P. A. Pantaleón, V. o. T. Phong, A. Jimeno-Pozo, and F. Guinea, Junctions and superconducting symmetry in twisted bilayer graphene, Phys. Rev. Lett. **131**, 016003 (2023).
[16] C. Lewandowski, E. Lantagne-Hurtubise, A. Thomson, S. Nadj-Perge, and J. Alicea, Andreev reflection spectroscopy in strongly paired superconductors, Phys. Rev. B **107**, L020502 (2023).
[17] P. P. Poduval and M. S. Scheurer, Vestigial singlet pairing in a fluctuating magnetic triplet superconductor and its implications for graphene superlattices, Nat. Commun. **15**, 1713 (2024).
[18] M. Christos, S. Sachdev, and M. S. Scheurer, Nodal band-off-diagonal superconductivity in twisted graphene superlattices, Nat. Commun. **14**, 7134 (2023).
[19] S. Van Loon and C. A. R. Sá de Melo, Topological two-band electron-hole superconductors with d-wave symmetry: Absence of Dirac quasiparticle annihilation in magic-angle twisted trilayer graphene, Phys. Rev. B **111**, 064515 (2025).
[20] Y.-Z. Chou, F. Wu, J. D. Sau, and S. Das Sarma, Acoustic-phonon-mediated superconductivity in rhombohedral trilayer graphene, Phys. Rev. Lett. **127**, 187001 (2021).
[21] A. Ghazaryan, T. Holder, M. Serbyn, and E. Berg, Unconventional superconductivity in systems with annular Fermi surfaces: Application to rhombohedral trilayer graphene, Phys. Rev. Lett. **127**, 247001 (2021).
[22] Y.-Z. You and A. Vishwanath, Kohn-Luttinger superconductivity and intervalley coherence in rhombohedral trilayer graphene, Phys. Rev. B **105**, 134524 (2022).
[23] S. Chatterjee, T. Wang, E. Berg, and M. P. Zaletel, Inter-valley coherent order and isospin fluctuation mediated superconductivity in rhombohedral trilayer graphene, Nat. Commun. **13**, 6013 (2022).
[24] A. Ghazaryan, T. Holder, E. Berg, and M. Serbyn, Multilayer graphenes as a platform for interaction-driven physics and topological superconductivity, Phys. Rev. B **107**, 104502 (2023).
[25] A. Jimeno-Pozo, H. Sainz-Cruz, T. Cea, P. A. Pantaleón, and F. Guinea, Superconductivity from electronic interactions and spin-orbit enhancement in bilayer and trilayer graphene, Phys. Rev. B **107**, L161106 (2023).
[26] W. Qin, C. Huang, T. Wolf, N. Wei, I. Blinov, and A. H. MacDonald, Functional renormalization group study of superconductivity in rhombohedral trilayer graphene, Phys. Rev. Lett. **130**, 146001 (2023).
[27] Z. Li, X. Kuang, A. Jimeno-Pozo, H. Sainz-Cruz, Z. Zhan, S. Yuan, and F. Guinea, Charge fluctuations, phonons, and superconductivity in multilayer graphene, Phys. Rev. B **108**, 045404 (2023).
[28] A. L. Szabó and B. Roy, Metals, fractional metals, and superconductivity in rhombohedral trilayer graphene, Phys. Rev. B **105**, L081407 (2022).
[29] Z. Dong, L. Levitov, and A. V. Chubukov, Superconductivity near spin and valley orders in graphene multilayers, Phys. Rev. B **108**, 134503 (2023).
[30] Z. Dong, É. Lantagne-Hurtubise, and J. Alicea, Superconductivity from spin-canting fluctuations in rhombohedral graphene, Phys. Rev. X **16**, 011055 (2026).
[31] T. Han, Z. Lu, Y. Yao, L. Shi, J. Yang, J. Seo, S. Ye, Z. Wu, M. Zhou, H. Liu, G. Shi, Z. Hua, K. Watanabe, T. Taniguchi, P. Xiong, L. Fu, and L. Ju, Signatures of chiral superconductivity in rhombohedral graphene, Nature (London) **643**, 654 (2025).
[32] H. D. Scammell, J. I. A. Li, and M. S. Scheurer, Theory of zero-field superconducting diode effect in twisted trilayer graphene, 2D Mater. **9**, 025027 (2022).
[33] Y.-Z. Chou, J. Zhu, and S. D. Sarma, Intravalley spin-polarized superconductivity in rhombohedral tetralayer graphene, Phys. Rev. B **111**, 174523 (2025).
[34] M. Geier, M. Davydova, and L. Fu, Chiral and topological superconductivity in isospin polarized multilayer graphene, Nat. Commun. **17**, 232 (2025).
[35] H. Yang and Y.-H. Zhang, Topological incommensurate Fulde-Ferrell-Larkin-Ovchinnikov superconductor and Bogoliubov Fermi surface in rhombohedral tetra-layer graphene, Phys. Rev. B, **112**, L020506 (2025).
[36] Q. Qin and C. Wu, Chiral finite-momentum superconductivity in the tetralayer graphene, Chinese Phys. Lett. **43**, 030708 (2026).
[37] G. Parra-Martinez, A. Jimeno-Pozo, V. Tien Phong, H. Sainz-Cruz, D. Kaplan, P. Emanuel, Y. Oreg, P. A. Pantaleon, J. A. Silva-Guillen, and F. Guinea, Band renormalization, quarter metals, and chiral superconductivity in rhombohedral tetralayer graphene, Phys. Rev. Lett. **135**, 136503 (2025).
[38] C. Yoon, T. Xu, Y. Barlas, and F. Zhang, Quarter metal superconductivity, Phys. Rev. Lett. **136**, 026603 (2026).
[39] M. Christos, P. M. Bonetti, and M. S. Scheurer, Finite-momentum pairing and superlattice superconductivity in valley-imbalanced rhombohedral graphene, arXiv:2503.15471.
[40] A. Jahin and S.-Z. Lin, Enhanced Kohn-Luttinger topological superconductivity in bands with nontrivial geometry, Phys. Rev. B **113**, 014504 (2026).
[41] J. May-Mann, T. Helbig, and T. Devakul, How pairing mechanism dictates topology in valley-polarized superconductors with Berry curvature, npj Quantum Mater. (2026).
[42] M. Kim, A. Timmel, L. Ju, and X.-G. Wen, Topological chiral superconductivity beyond pairing in a Fermi liquid, Phys. Rev. B **111**, 014508 (2025).
[43] S. Banerjee and M. S. Scheurer, Enhanced superconducting diode effect due to coexisting phases, Phys. Rev. Lett. **132**, 046003 (2024).
[44] P. H. Wilhelm, A. M. Läuchli, and M. S. Scheurer, Ideal Chern bands with strong short-range repulsion: Applications to correlated metals, superconductivity, and topological order, Phys. Rev. Res. **6**, 043240 (2024).
[45] J. C. Cuevas, A. Martín-Rodero, and A. L. Yeyati, Hamiltonian approach to the transport properties of superconducting quantum point contacts, Phys. Rev. B **54**, 7366 (1996).
[46] F. Zhang, B. Sahu, H. Min, and A. H. MacDonald, Band structure of *ABC*-stacked graphene trilayers, Phys. Rev. B **82**, 035409 (2010).
[47] M. Koshino and E. McCann, Trigonal warping and Berry's phase $N\pi$ in ABC-stacked multilayer graphene, Phys. Rev. B **80**, 165409 (2009).
[48] See Supplemental Material at http://link.aps.org/supplemental/10.1103/6qg4-cfgc for a detailed derivation of the tunneling current; symmetry analysis of the Andreev current; details on the different contributions to the Berry curvature of the superconductor; additional results for the finite-momentum single-**q** and three-**q** pairing states; discussion of a 1D toy model with a pair density wave.
[49] We here neglect an additional reflection symmetry σ_v for simplicity of the discussion.

[50] J. M. B. L. Dos Santos, N. M. R. Peres, and A. H. C. Neto, Graphene bilayer with a twist: Electronic structure, Phys. Rev. Lett. **99**, 256802 (2007).

[51] R. Bistritzer and A. H. MacDonald, Moiré bands in twisted double-layer graphene, Proc. Natl. Acad. Sci. USA **108**, 12233 (2011).

[52] K. P. Nuckolls, R. L. Lee, *et al.*, Quantum textures of the many-body wavefunctions in magic-angle graphene, Nature (London) **620**, 525 (2023).

[53] Y.-C. Tsui, M. He, Y. Hu, E. Lake, T. Wang, K. Watanabe, T. Taniguchi, M. P. Zaletel, and A. Yazdani, Direct observation of a magnetic-field-induced Wigner crystal, Nature (London) **628**, 287 (2024).

[54] S. Turkel, J. Swann, Z. Zhu, M. Christos, K. Watanabe, T. Taniguchi, S. Sachdev, M. S. Scheurer, E. Kaxiras, C. R. Dean, and A. N. Pasupathy, Orderly disorder in magic-angle twisted trilayer graphene, Science **376**, 193 (2022).

[55] Y. Liu, Z. Li, S. Jiang, M. Li, Y. Gu, K. Liu, Q. Shen, L. Liu, X. Liu, D. Guan, Y. Li, H. Zheng, C. Liu, K. Watanabe, T. Taniguchi, J. Jia, T. Li, G. Chen, J. Liu, C. Li, *et al.*, Electronic correlations in rhombohedral graphene at atomic scale, Phys. Rev. Lett. **135** 156401 (2025).

[56] R. Xu, L.-J. Yin, J.-B. Qiao, K.-K. Bai, J.-C. Nie, and L. He, Direct probing of the stacking order and electronic spectrum of rhombohedral trilayer graphene with scanning tunneling microscopy, Phys. Rev. B **91**, 035410 (2015).

[57] L.-J. Yin, Y.-Y. Zhou, L.-H. Tong, L.-J. Shi, Z. Qin, and L. He, Imaging Friedel oscillations in rhombohedral trilayer graphene, Phys. Rev. B **107**, L041404 (2023).

[58] Y. Liu, A. Gupta, Y. Choi, Y. Vituri, H. Stoyanov, J. Xiao, Y. Wang, H. Zhou, B. Barick, T. Taniguchi, K. Watanabe, B. Yan, E. Berg, A. F. Young, H. Beidenkopf, and N. Avraham, Visualizing incommensurate inter-valley coherent states in rhombohedral trilayer graphene, arXiv:2411.11163.